Data recording and neuron visualization

Auditory neurons were recorded and stained using thick-walled glass micropipettes filled with 5% Lucifer yellow and 0.5 M LiCl (resistance 100–150 MΩ). After recording, ganglia were processed conventionally and the stained neurons were identified under an ultraviolet fluorescence microscope. To record fictive motor activity, we placed a suction electrode on mesothoracic nerve 3A, which contains motor axons that innervate wing closer and opener muscles. A microphone (Audio-Technica AT853A) recorded sound produced by the cricket and an optoelectronic camera monitored wing movements. All data were transferred directly onto a computer through an AD board (Data Translation 2821 F8DI) with a sampling rate of 10 kHz per channel. We analysed data off-line using Neurolab[30] and Microsoft Excel 2000.

Received 19 February; accepted 23 May 2002; doi:10.1038/nature00919.

1. Creutzfeldt, O., Ojemann, G. & Lettich, E. Neuronal activity in the human temporal lobe II. Responses to the subjects own voice. *Exp. Brain Res.* **77,** 476–489 (1989).
2. Suga, N. & Schlegel, P. Neural attenuation of responses to emitted sounds in echolocating bats. *Science* **177,** 82–84 (1972).
3. Suga, N. & Shimozawa, T. Site of neural attenuation of responses to self-vocalized sounds in echolocating bats. *Science* **183,** 1211–1213 (1974).
4. Schuller, G. Vocalization influences auditory processing in collicular neurons of the CF-FM bat, *Rhinolophus ferrumequinum*. *J. Comp. Physiol. A* **132,** 39–46 (1979).
5. McCasland, J. S. & Konishi, M. Interaction between auditory and motor activities in an avian song control nucleus. *Proc. Natl Acad. Sci. USA* **78,** 7815–7819 (1981).
6. Müller-Preuss, P. & Ploog, D. Inhibition of auditory cortical neurons during phonation. *Brain Res.* **215,** 61–76 (1981).
7. Metzner, W. A possible neuronal basis for Doppler-shift compensation in echo-locating horseshoe bats. *Nature* **341,** 529–532 (1989).
8. Nocke, H. Physiological aspects of sound communication in crickets (*Gryllus campestris* L.). *J. Comp. Physiol. A* **80,** 141–162 (1972).
9. Michel, K. Das Tympanalorgan von *Gryllus bimaculatus* DeGeer (Saltatoria, Gryllidae). *Z. Morph. Tiere* **77,** 285–315 (1974).
10. Schildberger, K., Wohlers, D. W. & Huber, F. in *Cricket Behaviour and Neurobiology* (eds Huber, F., Moore, T. E. & Loher, T. E.) 423–458 (Cornell Univ. Press, Ithaca/London, 1989).
11. Jones, M. D. R. & Dambach, M. Response to sound in crickets without tympanal organs (*Gryllus campestris* L.). *J. Comp. Physiol. A* **87,** 89–98 (1973).
12. Suga, N. & Jen, P. Peripheral control of acoustic signals in the auditory system of echolocating bats. *J. Exp. Biol.* **62,** 277–311 (1975).
13. Borg, E. & Counter, S. The middle-ear muscles. *Sci. Am.* **261 (August),** 62–68 (1989).
14. Narins, P. M. Reduction of tympanic membrane displacement during vocalization of the arboreal tree frog, *Eleutherodactylus coqui*. *J. Acoust. Soc. Am.* **91,** 3551–3557 (1992).
15. Hennig, R. M. *et al.* Auditory threshold change in singing cicadas. *J. Exp. Biol.* **187,** 45–55 (1994).
16. Poulet, J. F. A. & Hedwig, B. Tympanic membrane oscillations and auditory receptor activity in the stridulating cricket *Gryllus bimaculatus*. *J. Exp. Biol.* **204,** 1281–1293 (2001).
17. Clarac, F. & Cattaert, D. Invertebrate presynaptic inhibition and motor control. *Exp. Brain Res.* **112,** 163–180 (1996).
18. Hardt, M. & Watson, A. H. D. Distribution of input and output synapses on the central branches of bushcricket and cricket auditory afferent neurones: immunocytochemical evidence for GABA and glutamate in different populations of presynaptic boutons. *J. Comp. Neurol.* **403,** 281–294 (1999).
19. Pollack, G. S. Selective attention in an insect auditory neuron. *J. Neurosci.* **8,** 2635–2639 (1988).
20. Sobel, E. C. & Tank, D. W. *In vivo* Ca^{2+} dynamics in a cricket auditory neuron: an example of chemical computation. *Science* **263,** 823–826 (1994).
21. Givois, V. & Pollack, G. S. Sensory habituation of auditory receptor neurons: implications for sound localization. *J. Exp. Biol.* **203,** 2529–2537 (2000).
22. von Holst, E. & Mittelstaedt, H. Das reafferenzprinzip. (Wechselwirkungen zwischen zentralnervensystem und peripherie.). *Naturwissenschaften* **37,** 464–476 (1950).
23. Sperry, R. W. Neural basis of the spontaneous optokinetic response produced by visual inversion. *J. Comp. Physiol. Psych.* **43,** 482–489 (1950).
24. Zaretsky, M. & Rowell, C. H. F. Saccadic suppression by corollary discharge in the locust. *Nature* **280,** 583–585 (1979).
25. Bell, C. C. An efference copy which is modified by reafferent input. *Science* **214,** 450–453 (1981).
26. Guthrie, B. L., Porter, J. D. & Sparks, D. L. Corollary discharge provides accurate eye position information to the oculomotor system. *Science* **221,** 1193–1195 (1983).
27. Sillar, K. T. & Roberts, A. A neuronal mechanism for sensory gating during locomotion in a vertebrate. *Nature* **331,** 262–265 (1988).
28. Bell, C. C. in *Comparative Physiology of Sensory Systems* (eds Bolis, L., Keynes, R. D. & Maddrell, S. H. P.) 636–647 (Cambridge Univ. Press, Cambridge, 1984).
29. Hedwig, B. Control of cricket stridulation by a command neuron: efficacy depends on the behavioural state. *J. Neurophysiol.* **83,** 712–722 (2000).
30. Knepper, M. & Hedwig, B. NEUROLAB, a PC-program for the processing of neurobiological data. *Comp. Methods Programs Biomed.* **52,** 75–77 (1997).

Acknowledgements

We thank M. Burrows, T. Matheson and S. Rogers for comments on the manuscript. This work was supported by a Biotechnology and Biological Sciences Research Council (BBSRC) studentship and grants from the Wellcome Trust and the Royal Society.

Competing interests statement

The authors declare that they have no competing financial interests.

Correspondence and requests for materials should be addressed to J.P. (e-mail: jfap2@cam.ac.uk) or B.H. (e-mail: bh202@cam.ac.uk)

Mechanism of magnesium activation of calcium-activated potassium channels

Jingyi Shi*, Gayathri Krishnamoorthy*, Yanwu Yang†, Lei Hu*, Neha Chaturvedi*, Dina Harilal*, Jun Qin† & Jianmin Cui*

* *Cardiac Bioelectricity Research and Training Center and Department of Biomedical Engineering, Case Western Reserve University, Cleveland, Ohio 44106-7207, USA*

† *Structural Biology Program, Lerner Research Institute, The Cleveland Clinic Foundation, Cleveland, Ohio 44195, USA*

Large-conductance (BK type) Ca^{2+}-dependent K^+ channels are essential for modulating muscle contraction and neuronal activities such as synaptic transmission and hearing[1–5]. BK channels are activated by membrane depolarization and intracellular Ca^{2+} and Mg^{2+} (refs 6–10). The energy provided by voltage, Ca^{2+} and Mg^{2+} binding are additive in activating the channel, suggesting that these signals open the activation gate through independent pathways[9,11]. Here we report a molecular investigation of a Mg^{2+}-dependent activation mechanism. Using a combined site-directed mutagenesis and structural analysis, we demonstrate that a structurally new Mg^{2+}-binding site in the RCK/Rossman fold domain—an intracellular structural motif that immediately follows the activation gate S6 helix[12–15]—is responsible for Mg^{2+}-dependent activation. Mutations that impair or abolish Mg^{2+} sensitivity do not affect Ca^{2+} sensitivity, and vice versa. These results indicate distinct structural pathways for Mg^{2+}- and Ca^{2+}-dependent activation and suggest a possible mechanism for the coupling between Mg^{2+} binding and channel opening.

The energetically separate Ca^{2+}- and Mg^{2+}-dependent activation pathways suggest that each pathway may involve distinct structural components of the channel. Previous results suggest that a low-affinity, divalent cation-binding site that is responsible for Mg^{2+}-dependent activation may be located in the amino-terminal core of mouse Slo1 (mSlo1) subunits[9,16] (Fig. 1a). Thus, the Mg^{2+}-binding site is distinct from the high-affinity Ca^{2+}-binding site that has been proposed to reside in the carboxy terminal tail[17–19] (Fig. 1a). The RCK domain is an intracellular motif of the core that immediately follows the activation gate S6 helix[12–15] (Fig. 1a). It is conserved among BK channels, various prokaryotic K^+ channels and TrkA proteins (which regulate K^+ conductance[12]). The X-ray crystal structure of the RCK domain of the *Escherichia coli* Kch channel indicates that this domain may contain a ligand-binding site at its N-terminal half[12]. To examine whether the N terminus of the mSlo1 RCK domain contains the low-affinity metal-binding site, we first studied chimaeric channels between mSlo1 and its homologue mSlo3 (ref. 20)—the activation of which is insensitive to Mg^{2+}, although it also contains the RCK domain[9,12] (Fig. 1). Comparing the sequence of mSlo1 with mSlo3, it is obvious that differences scatter within the N-terminal region of the RCK domain (Fig. 2a). If these differences occur in the metal-binding site, they may result in the difference in Mg^{2+} sensitivity between these two channels. Figure 1c (left panel) shows that the conductance–voltage (G–V) relation of chimaera C31-I (see Methods for definition of chimaeras) shifted less than that of mSlo1 when intracellular Mg^{2+} concentration ($[Mg^{2+}]_i$) increased from 0 to 10 mM, whereas the increase of $[Mg^{2+}]_i$ caused no change in the G–V relation of C31-II. The total loss of Mg^{2+} sensitivity in C31-II is consistent with the idea that the sequence of mSlo3 in this region may have destroyed the metal-binding site. On the other hand, chimaera C13 was activated by Mg^{2+} (Fig. 1c, right panel), indicating that this region in mSlo1 is sufficient to restore Mg^{2+} sensitivity in mSlo3. Figure 1d

compares the free energy provided by Mg^{2+} binding towards the activation of mSlo1, mSlo3 and chimaeric channels[9,11] (see Methods and Supplementary Information), and quantitatively demonstrates that the mSlo1 sequence at the N terminus of the RCK domain is essential for Mg^{2+}-dependent activation.

To identify individual amino acids that are important for Mg^{2+}-dependent activation we studied the effects of site-directed mutations on the Mg^{2+} sensitivity of mSlo1 channels. The core structure of the RCK domain adopts a Rossmann fold with a six-stranded parallel β-sheet (βA–βF) and α-helices (αA–αE) on both sides[12]. Figure 2a shows the sequence alignment of the N terminus of the RCK domain that includes βA–αC in mSlo1, *Drosophila* Slo (dSlo)[21], mSlo3 and *E. coli* Kch[22] channels. The activation of dSlo channels has a similar Mg^{2+} sensitivity as that of mSlo1 (data not shown). Residues that are conserved in mSlo1 and dSlo but not in mSlo3 (Fig. 2a) are probably responsible for the difference in Mg^{2+} sensitivities among these channels. Therefore, in one series of mutations these residues in mSlo1 were mutated into the corresponding amino acids in mSlo3, either individually or in combination (Fig. 2b). In another series of mutations, oxygen-containing residues that are conserved in mSo1 and dSlo—which may possibly be Mg^{2+}-coordinating—were mutated into Ala or other amino acids as indicated in Fig. 2b. The effects of these mutations on Mg^{2+} sensitivity show a clear pattern with regard to the position of mutated residues (Fig. 2b). Mutations at the interloop connecting βA and αA (H350N), both N- and C-termini of βB (E374A, H379G), and towards the N terminus of βC (T396A, Q397C and E399N) reduced Mg^{2+} sensitivity, whereas mutations at other segments had no significant effects on Mg^{2+} sensitivity. Most notably, a change in either of two residues, E374A or E399N, completely abolished Mg^{2+}-dependent activation at 110 μM $[Ca^{2+}]_i$ (Fig. 2c). The large effect of the mutations E374A and E399N on Mg^{2+} sensitivity was not accompanied by any change in Ca^{2+}-dependent activation or activation in the absence of Ca^{2+} and Mg^{2+} (Fig. 2c), suggesting that no gross change of channel structure had resulted from these mutations. E374 is conserved among mSlo1, dSlo and mSlo3, whereas E399 is conserved in mSlo1 and dSlo but not in mSlo3 (Fig. 2a), which explains why the chimaera

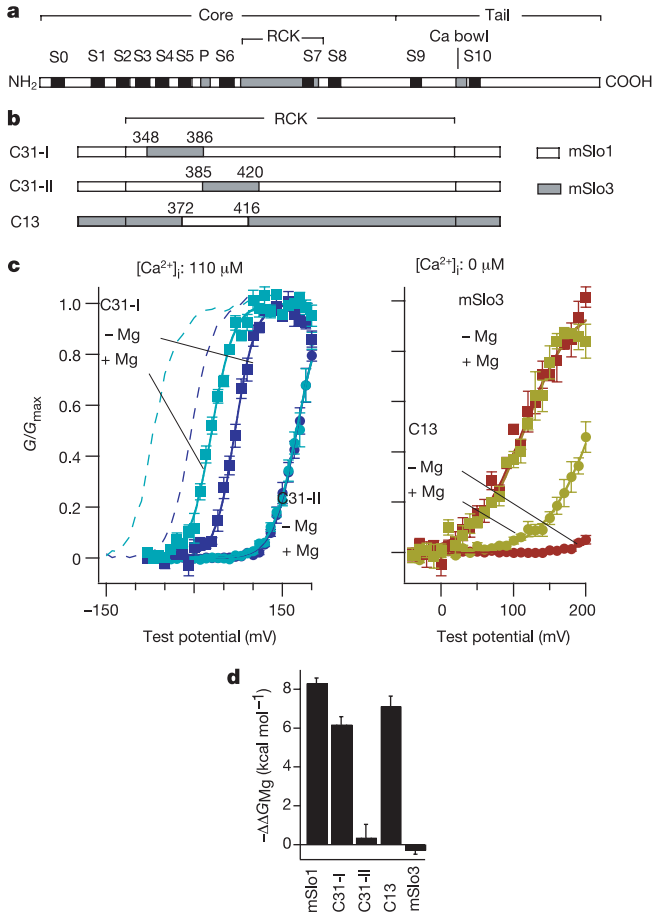

Figure 1 Results of chimaeric channels. **a**, The Slo polypeptide. S0–S6, transmembrane segments; P, pore loop; S7–S10, cytoplasmic hydrophobic segments; Ca bowl, putative high-affinity Ca^{2+}-binding site[18]. **b**, Constructs of chimaeric channels C31-I, C31-II and C13. Numbers indicate the position in mSlo1 where the substitution starts and ends. **c**, Mean *G–V* relations of C31-I, C31-II, mSlo3 and C13 at 0 and 10 mM $[Mg^{2+}]_i$ ($n = 5$–6 patches). Dashed lines are *G–V* relations of mSlo1 for comparison (Supplementary Information). **d**, Free energy provided by Mg^{2+} binding towards the activation of channels when $[Mg^{2+}]_i$ increases from 0 to 10 mM.

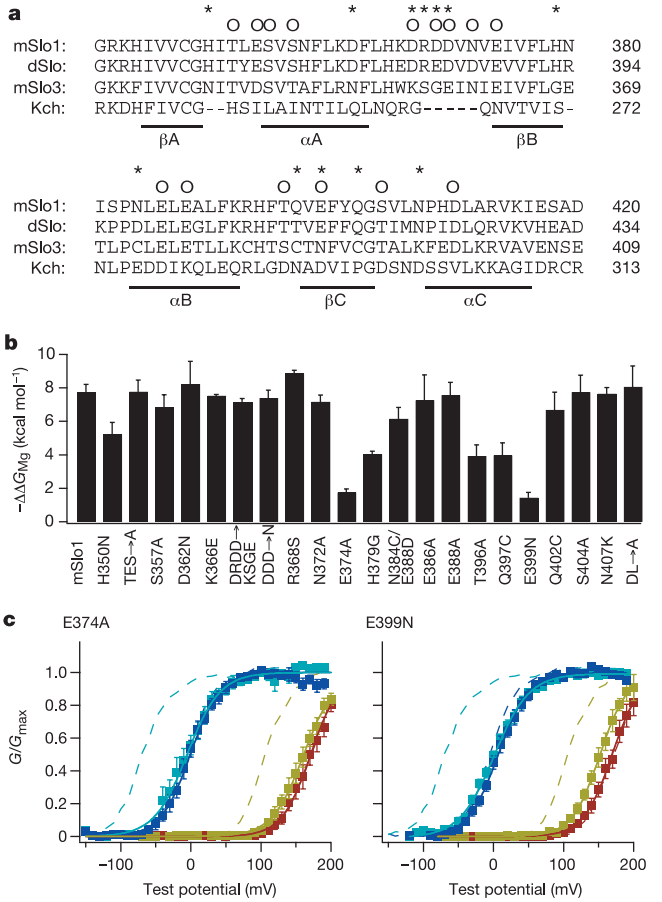

Figure 2 Results of site-directed mutations. **a**, Sequence alignment of part of the RCK domain in mSlo1, dSlo, mSlo3 and *E. coli* Kch channels[12]. Underlines indicate amino acids that form α-helices (αA–αC) and β-strands (βA–βC). Numbers indicate the position of the far right residues in the primary sequence of their respective proteins. Asterisk, residues that are conserved in mSlo1 and dSlo, but not in mSlo3; O, oxygen-containing residues that are conserved in mSlo1 and dSlo. **b**, Free energy provided by Mg^{2+} binding in activating the wild type and mutant mSlo1 channels when $[Mg^{2+}]_i$ increases from 0 to 10 mM. Free energy was measured at 0 $[Ca^{2+}]_i$ except for TES → A and H379G (measured at 110 μM $[Ca^{2+}]_i$). For single mutations, the original amino acid of mSlo1, its position, and the amino acid that it is changed to are indicated. TES → A, T352, E354 and S355 are changed to A; DRDD → KSGE, DRDD (positions 367–370) are changed to KSGE; DDD → N, D367, D369 and D370 are changed to N; N384C/E388D, a double mutant N384C and E388D; DL → A, D410 and L411 are changed to A. $n = 3$–6 patches for each channel. **c**, Mean *G–V* relations of E374A and E399N channels. $[Mg^{2+}]_i$ and $[Ca^{2+}]_i$ are colour-coded as in Fig. 1c. Dashed lines are *G–V* relations of mSlo1 for comparison (Supplementary Information).

C31-II lost Mg^{2+}-sensitivity but C31-I did not (Fig. 1). These results suggest that residues E374 and E399 are part of the low-affinity, metal-binding site, which are exposed to the aqueous solution and are coordinated to the bound Mg^{2+} ion. Therefore, mutation of these residues should have little impact on the channel structure, but should significantly affect Mg^{2+} binding.

Figure 3 shows the structure of the N terminus of the RCK domain of *E. coli* Kch channels[12] in which the residues at positions corresponding to E374, Q397, E399 and H379 of mSlo1 (N267, N289, D292 and S272 in Kch; Fig. 2a) are substituted by mSlo1 counterparts. A metal-binding site with a bound Mg^{2+} ion is shown as the result of energy minimization. The Mg^{2+} ion is coordinated by the side chains of E374 and E399 (located at the N terminus of two adjacent β-strands, βB and βC), and Q397 (in the loop connecting the N terminus of βC with αB). The main chain carbonyl oxygen of Q397 also coordinates to the Mg^{2+} ion (Fig. 3). These results are consistent with mutational results (Figs 1 and 2). However, the location of the site was unexpected because in other proteins with a Rossman fold—such as the response regulator of bacterial chemotaxis, CheY[23], and integrin domain A[24]—the ligand-binding site is always formed by loops connecting the C terminus of the parallel β-strands to helices[25] (indicated by the arrow in Fig. 3). Nevertheless, such an organization of metal coordination in mSlo1 is comparable to that found in CheY, in which three Asp side chains and one backbone carbonyl are coordinated to the Mg^{2+} ion[23]. The metal site in CheY selectively binds divalent or trivalent cations but does not discriminate between metals on the basis of their size[26]. Similarly, the low-affinity metal site in mSlo1 channels binds Mg^{2+} with a comparable affinity as Ca^{2+} at the millimolar range[9,10], which is around the physiological intracellular Mg^{2+} concentration[27]. Therefore, in a typical cell, this site is essentially a Mg^{2+}-binding site.

The results of structural analysis reveal that Q397 is one of the Mg^{2+}-coordinating residues. The mutation Q397C reduced Mg^{2+} sensitivity of the channel but did not completely abolish it at 0 or 110 μM $[Ca^{2+}]_i$ (Fig. 4a). Thus, the coordination by the side chain of Q397 is probably replaced either by a water molecule or the thiol group of Cys, and thus maintains some Mg^{2+} sensitivity. When an Asp residue, which is also negatively charged but with a shorter side chain, replaced E374 (E374D) or E399 (E399D), the channel remained sensitive to Mg^{2+} (Fig. 4a), indicating that Mg^{2+} could still bind to the site. However, Mg^{2+} sensitivity was reduced by both mutations owing to the change in size of the side chain. The effects of E374D and E399D are not equal (Fig. 4a). This is possibly due to the coordination of the main chain carbonyl of Q397 pulling the metal closer to the backbone of βC (Fig. 3) and thus helping to better accommodate the space change caused by E399D. Notably, when E374 or E399 is replaced by non-charged (Ala or Gln) or positively charged residues (Arg), an increase of $[Mg^{2+}]_i$ from 0 to 10 mM at 0 $[Ca^{2+}]_i$ still activated the channel to a small but observable extent (Figs 2c and 4a). As these mutations should destroy the low-affinity metal-binding site, such a residual sensitivity to Mg^{2+} is probably derived from Mg^{2+} binding to the high-affinity Ca^{2+} site, which subsequently activated the channel. Consistent with this idea, at 110 μM $[Ca^{2+}]_i$, which is saturating for the high-affinity Ca^{2+} site[8], Mg^{2+} could no longer activate these mutant channels (Figs 2c and 4a). This idea is further supported by the result that the mSlo3 channel, which also lacks Ca^{2+} sensitivity, was not activated by Mg^{2+} at 0 $[Ca^{2+}]_i$ (ref. 9) (Fig. 1c).

Figure 4b shows that of the mutations that impaired or abolished Mg^{2+} sensitivity, none affected the free energy provided by Ca^{2+} binding towards the activation of the channel when $[Ca^{2+}]_i$ increased from 0 to 110 μM, at an intracellular Mg^{2+} concentration

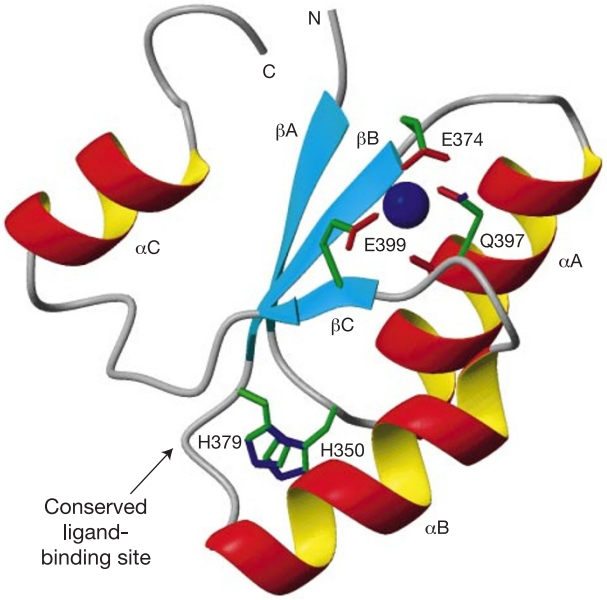

Figure 3 Structure of the Mg^{2+}-binding site. The blue sphere indicates a bound metal ion. Residues are labelled with their position in mSlo1. The conserved ligand-binding site in most other ligand-binding proteins with a Rossman fold is labelled with an arrow.

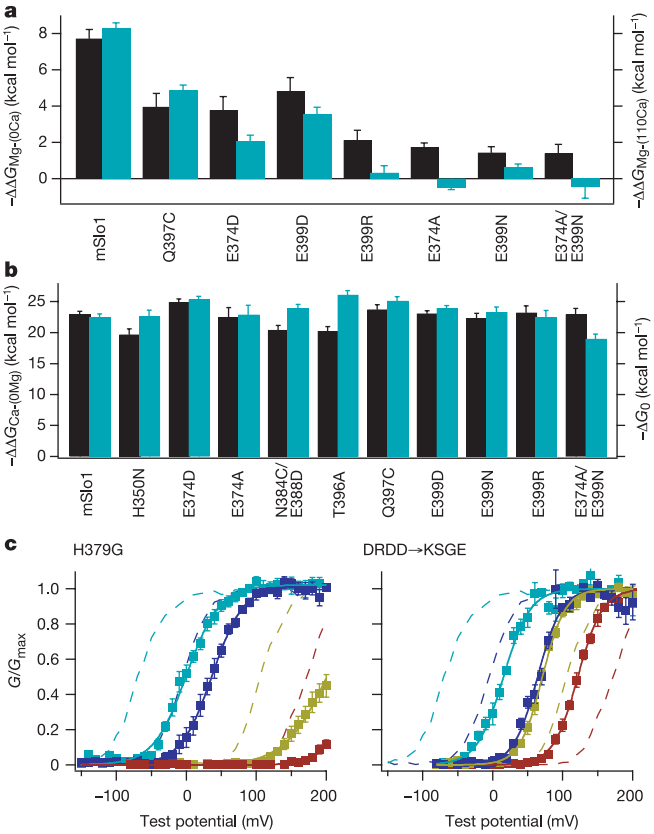

Figure 4 Results of site-directed mutations that affect channel gating. **a**, Mutations on Mg^{2+}-coordinating residues. The graph shows the free energy provided by Mg^{2+} binding towards the activation of channels when $[Mg^{2+}]_i$ increases from 0 to 10 mM, measured at 0 (left *y* axis, black columns) and 110 μM (right *y* axis, green columns) $[Ca^{2+}]_i$ ($\Delta\Delta G_{Mg\text{-}(Ca)}$). **b**, Mutations affecting Mg^{2+} sensitivity. The graph shows the free energy increase in the absence of Ca^{2+} and Mg^{2+} at 0 mV (ΔG_0, green columns), and the free energy provided by Ca^{2+} binding towards the activation of channels when $[Ca^{2+}]_i$ increases from 0 to 110 μM at 0 $[Mg^{2+}]_i$ ($\Delta\Delta G_{Ca\text{-}(0Mg)}$, black columns). **c**, Mean *G–V* relations of H379G and DRDD/KSGE channels. $[Mg^{2+}]_i$ and $[Ca^{2+}]_i$ are colour-coded as in Fig. 1c. Dashed lines are *G–V* relations of mSlo1 for comparison. $n = 4$–7 patches for each mutation.

of 0 ($\Delta\Delta G_{Ca\text{-}(0Mg)}$; see also Methods). The measurement of $\Delta\Delta G_{Ca\text{-}(0Mg)}$ for mutation H379G, which also reduced Mg^{2+} sensitivity (Fig. 2b), is not shown on Fig. 4b because the *G–V* relation was shifted to right and could not be measured accurately (Fig. 4c). Instead, a value of $\Delta\Delta G_{Ca-(0Mg)} = 12.5 \pm 0.7\,kcal\,mol^{-1}$ ($n = 6$) was measured between 2 and 110 μM $[Ca^{2+}]_i$ and compared with that of mSlo1 channels ($12.0 \pm 0.4\,kcal\,mol^{-1}$, $n = 3$); this treatment showed no significant difference. Therefore, the structural components that are affected by these mutations are involved in Mg^{2+}- but not Ca^{2+}-dependent activation. On the other hand, when residues in the interloop connecting αA–βB of mSlo1 were mutated to corresponding mSlo3 residues (DRDD → KSGE, Figs 2a and 3), the free energy provided by Ca^{2+}-binding towards the activation of the channel was reduced to about one-third of that for mSlo1 (Fig. 4c). This result indicates an important role of this loop in Ca^{2+}-dependent activation. However, although this loop is spatially close to the Mg^{2+}-binding site, mutation DRDD → KSGE had no effect on Mg^{2+} sensitivity (Fig. 2b). Similarly, when the tail domain of mSlo1 is substituted by the tail of mSlo3, the channel loses Ca^{2+} sensitivity but retains an intact Mg^{2+} sensitivity[9,18]. These results indicate that the tail domain and the interloop connecting αA–βB in the RCK domain may be involved in Ca^{2+}- but not Mg^{2+}-dependent activation. Thus, distinct structural components are responsible for Ca^{2+}- and Mg^{2+}-dependent activation of BK channels. Not only are the binding sites different, but also the energy provided by metal binding affects different sets of local conformational changes that eventually lead to channel opening.

The results from chimaera studies (Fig. 1) demonstrate that only a small fragment of mSlo1 is necessary and sufficient for restoring Mg^{2+} sensitivity in mSlo3 channels despite numerous other amino acid sequence differences between the two. Within this fragment, H350, H379 and N384 are located in the conserved active site of other proteins that adopt a Rossman fold[12,25] (arrow in Fig. 3). Mutations of these residues affect Mg^{2+} sensitivity (Fig. 2b). These results mark the conserved active site as the only area away from the Mg^{2+} binding site that is important for Mg^{2+} sensitivity. These residues do not act independently to affect Mg^{2+} sensitivity, because the reduction of free energy provided by Mg^{2+} binding towards the activation of the channel caused by each individual mutation does not add up to the reduction caused by chimaera C31-I, which includes all of these individual mutations (Figs 1c and 2b)[28]. Consistent with these results, structural analysis indicates that the side chains of H350 and H379 are close to each other, possibly interacting by stacking of their aromatic rings (Fig. 3). Thus, it appears that in BK channels Mg^{2+} binding at the N terminus of β-strands places an energetic constraint on the conformational change at the conserved active site located at the C terminus of β-strands, thereby activating the channel. Given the close proximity between the RCK domain and the S6 helix that forms the activation gate[13–15] (Fig. 1a), it is possible that the conserved active site directly interacts with the activation gate. □

Methods

Mutagenesis and expression

All channel constructs were made from the mbr5 clone of mSlo1 (ref. 16) and the complementary DNA of mSlo3 (ref. 20). In C31-I, amino acids 348–386 of mSlo1 are substituted by amino acids 337–375 of mSlo3. In C31-II, amino acids 385–420 of mSlo1 are substituted by amino acids 374–409 of mSlo3. In C13, amino acids 361–405 of mSlo3 are substituted by amino acids 372–416 of mSlo1. The polymerase chain reaction (PCR)-amplified regions of all mutants were verified by sequencing. A PCR error in chimaera C31-I resulted in an additional mutation V553G. As V553 is not conserved between the Mg^{2+}-sensitive mSlo1 and dSlo, the additional mutation was not corrected. RNA was transcribed *in vitro* with T3 polymerase (Ambion). We injected 0.05–50 ng of RNA into each *Xenopus laevis* oocyte 2–6 days before recording.

Electrophysiology

Macroscopic currents were recorded from inside-out patches formed with borosilicate pipettes of 0.9–1.8 MΩ resistance. Data were acquired using an Axopatch 200-B patch clamp amplifier (Axon Instruments) and pulse acquisition software (HEKA Electronik). Records were digitized at 20-μs intervals and low-pass-filtered at 10 KHz with the 4 pole Bessel filter of Axopatch. The pipette solution contained (in mM): 140 potassium methanesulphonic acid, 20 HEPES, 2 KCl, 2 $MgCl_2$, pH 7.20. The basal internal solution contained (in mM): 140 potassium methanesulphonic acid, 20 HEPES, 2 KCl, 1 EGTA, pH 7.20. The '0 $[Ca^{2+}]_i$' solution was the same as the basal internal solution except that it contained 5 mM EGTA, having a free $[Ca^{2+}]_i$ of approximately 0.5 nM that was too low to affect mSlo1 channel activation[8]. $CaCl_2$ and $MgCl_2$ were added to internal solutions to give the appropriate free $[Ca^{2+}]_i$ and $[Mg^{2+}]_i$ (ref. 9). We obtained all recordings at room temperature (22–24 °C).

Analysis

Relative conductance was determined by measuring tail current amplitudes at −50 mV. *G–V* relations were fitted with the Boltzmann distribution $G/G_{max} = 1/[1 + \exp(\Delta G_{Act}/kT)]$, where k is Boltzmann's constant, T is absolute temperature, and ΔG_{Act} is the free energy change of channel opening. Because voltage, Ca^{2+} and Mg^{2+} open the activation gate independently, ΔG_{Act} is the sum of energy increase provided by voltage ($\Delta G_V = -zeV$, where e is the elementary charge and z is the number of equivalent charges), Ca^{2+} and Mg^{2+} binding (ΔG_{Ca}, ΔG_{Mg}), and that in the absence of Ca^{2+} and Mg^{2+} at 0 mV (ΔG_0)[9,11]; so $\Delta G_{Act} = \Delta G_V + \Delta G_{Ca} + \Delta G_{Mg} + \Delta G_0$.

The change in Ca^{2+}- or Mg^{2+}-binding contribution to ΔG_{Act} as a result of an increase of $[Ca^{2+}]_i$ or $[Mg^{2+}]_i$ ($\Delta\Delta G_{Ca}$ or $\Delta\Delta G_{Mg}$) was then calculated based on the shift of the *G–V* relation: $\Delta\Delta G_{Ca} = -\Delta(zeV_{1/2})$ or $\Delta\Delta G_{Mg} = -\Delta(zeV_{1/2})$, where $V_{1/2}$ is the voltage at half maximum of the *G–V* relation. Error bars in all figures show standard error of means.

Molecular modelling

The structure of the RCK domain was generated by residual replacement based on the coordinates of the crystal structure of the RCK domain from the *E. coli* K^+ channel[12]. Magnesium ion was manually docked onto the potential Mg^{2+}-binding site as derived from mutation results. Then, the energy minimization was performed by fixing all backbone atoms and using the Discover Package with Insight II interface (Molecular Simulation). Structural diagrams were made using MolMol[29].

Received 25 April; accepted 17 June 2002; doi:10.1038/nature00941.

1. Brenner, R. *et al.* Vasoregulation by the β1 subunit of the calcium-activated potassium channel. *Nature* **407,** 870–876 (2000).
2. Robitaille, R., Garcia, M. L., Kaczorowski, G. J. & Charlton, M. P. Functional colocalization of calcium and calcium-gated potassium channels in control of transmitter release. *Neuron* **11,** 645–655 (1993).
3. Isaacson, J. S. & Murphy, G. J. Glutamate-mediated extrasynaptic inhibition: direct coupling of NMDA receptors to Ca(2 +)-activated K^+ channels. *Neuron* **31,** 1027–1034 (2001).
4. Fettiplace, R. & Fuchs, P. A. Mechanisms of hair cell tuning. *Annu. Rev. Physiol.* **61,** 809–834 (1999).
5. Rosenblatt, K. P., Sun, Z. P., Heller, S. & Hudspeth, A. J. Distribution of Ca^{2+}-activated K^+ channel isoforms along the tonotopic gradient of the chicken's cochlea. *Neuron* **19,** 1061–1075 (1997).
6. Pallotta, B. S., Magleby, K. L. & Barrett, J. N. Single channel recordings of Ca^{2+}-activated K^+ currents in rat muscle cell culture. *Nature* **293,** 471–474 (1981).
7. Marty, A. Ca-dependent K channels with large unitary conductance in chromaffin cell membranes. *Nature* **291,** 497–500 (1981).
8. Cui, J., Cox, D. H. & Aldrich, R. W. Intrinsic voltage dependence and Ca^{2+} regulation of mslo large conductance Ca-activated K^+ channels. *J. Gen. Physiol.* **109,** 647–673 (1997).
9. Shi, J. & Cui, J. Intracellular Mg(2 +) enhances the function of BK-type Ca(2 +)-activated K(+) channels. *J. Gen. Physiol.* **118,** 589–606 (2001).
10. Zhang, X., Solaro, C. R. & Lingle, C. J. Allosteric regulation of BK channel gating by Ca(2+) and Mg(2 +) through a nonselective, low affinity divalent cation site. *J. Gen. Physiol.* **118,** 607–636 (2001).
11. Cui, J. & Aldrich, R. W. Allosteric linkage between voltage and Ca(2 +)-dependent activation of BK-type mslo1 K(+) channels. *Biochemistry* **39,** 15612–15619 (2000).
12. Jiang, Y., Pico, A., Cadene, M., Chait, B. T. & MacKinnon, R. Structure of the RCK domain from the *E. coli* K^+ channel and demonstration of its presence in the human BK channel. *Neuron* **29,** 593–601 (2001).
13. Yellen, G. The moving parts of voltage-gated ion channels. *Q. Rev. Biophys.* **31,** 239–295 (1998).
14. Perozo, E., Cortes, D. M. & Cuello, L. G. Structural rearrangements underlying K^+-channel activation gating. *Science* **285,** 73–78 (1999).
15. Johnson, J. P. Jr & Zagotta, W. N. Rotational movement during cyclic nucleotide-gated channel opening. *Nature* **412,** 917–921 (2001).
16. Butler, A., Tsunoda, S., McCobb, D. P., Wei, A. & Salkoff, L. mSlo, a complex mouse gene encoding 'maxi' calcium-activated potassium channels. *Science* **261,** 221–224 (1993).
17. Wei, A., Solaro, C., Lingle, C. & Salkoff, L. Calcium sensitivity of BK-type KCa channels determined by a separable domain. *Neuron* **13,** 671–681 (1994).
18. Schreiber, M., Yuan, A. & Salkoff, L. Transplantable sites confer calcium sensitivity to BK channels. *Nature Neurosci.* **2,** 416–421 (1999).
19. Bian, S., Favre, I. & Moczydlowski, E. Ca^{2+}-binding activity of a COOH-terminal fragment of the *Drosophila* BK channel involved in Ca^{2+}-dependent activation. *Proc. Natl Acad. Sci. USA* **98,** 4776–4781 (2001).
20. Schreiber, M. *et al.* Slo3, a novel pH-sensitive K^+ channel from mammalian spermatocytes. *J. Biol. Chem.* **273,** 3509–3516 (1998).
21. Adelman, J. P. *et al.* Calcium-activated potassium channels expressed from cloned complementary DNAs. *Neuron* **9,** 209–216 (1992).
22. Milkman, R. An *Escherichia coli* homologue of eukaryotic potassium channel proteins. *Proc. Natl Acad. Sci. USA* **91,** 3510–3514 (1994).
23. Stock, J. B., Surette, M. G., McCleary, W. R. & Stock, A. M. Signal transduction in bacterial chemotaxis. *J. Biol. Chem.* **267,** 19753–19756 (1992).
24. Lee, J. O., Rieu, P., Arnaout, M. A. & Liddington, R. Crystal structure of the A domain from the alpha subunit of integrin CR3 (CD11b/CD18). *Cell* **80,** 631–638 (1995).
25. Brandeen, C. I. Relation between structure and function of alpha/beta-proteins. *Q. Rev. Biophys.* **13,** 317–338 (1980).

26. Needham, J. V., Chen, T. Y. & Falke, J. J. Novel ion specificity of a carboxylate cluster Mg(II) binding site: strong charge selectivity and weak size selectivity. *Biochemistry* **32,** 3363–3367 (1993).
27. Flatman, P. W. Mechanisms of magnesium transport. *Annu. Rev. Physiol.* **53,** 259–271 (1991).
28. Horovitz, A. & Fersht, A. R. Strategy for analysing the co-operativity of intramolecular interactions in peptides and proteins. *J. Mol. Biol.* **214,** 613–617 (1990).
29. Koradi, R., Billeter, M. & Wuthrich, K. MOLMOL: a program for display and analysis of macromolecular structures. *J. Mol. Graph.* **14,** 51–55 (1996).

Supplementary Information accompanies the paper on *Nature*'s website (http://www.nature.com/nature).

Acknowledgements

The mSlo1 and mSlo3 clones were provided by L. Salkoff. We thank S. Chen, S. W. Jones and R. Aldrich for comments on the manuscript. This work was supported by grants from the NIH (to J.Q. and J.C.), the American Heart Association and the Whitaker Foundation (to J.C.).

Competing interests statement

The authors declare that they have no competing financial interests.

Correspondence and requests for materials should be addressed to J.C. (e-mail: jxc93@cwru.edu).

Multiple regulatory sites in large-conductance calcium-activated potassium channels

Xiao-Ming Xia, Xuhui Zeng & Christopher J. Lingle

Department of Anesthesiology, Washington University School of Medicine, Box 8054, St. Louis, Missouri 63110, USA

Large conductance, Ca^{2+}- and voltage-activated K^+ channels (BK) respond to two distinct physiological signals—membrane voltage and cytosolic Ca^{2+} (refs 1, 2). Channel opening is regulated by changes in Ca^{2+} concentration spanning 0.5 μM to 50 mM (refs 2–5), a range of Ca^{2+} sensitivity unusual among Ca^{2+}-regulated proteins. Although voltage regulation arises from mechanisms shared with other voltage-gated channels[6–8], the mechanisms of Ca^{2+} regulation remain largely unknown. One potential Ca^{2+}-regulatory site, termed the 'Ca^{2+} bowl', has been located to the large cytosolic carboxy terminus[9–11]. Here we show that a second region of the C terminus, the RCK domain (regulator of conductance for K^+ (ref. 12)), contains residues that define two additional regulatory effects of divalent cations. One site, together with the Ca^{2+} bowl, accounts for all physiological regulation of BK channels by Ca^{2+}; the other site contributes to effects of millimolar divalent cations that may mediate physiological regulation by cytosolic Mg^{2+} (refs 5, 13). Independent regulation by multiple sites explains the large concentration range over which BK channels are regulated by Ca^{2+}. This allows BK channels to serve a variety of physiological roles contingent on the Ca^{2+} concentration to which the channels are exposed[14,15].

A recent advance in understanding the regulation of BK channels by Ca^{2+} was the demonstration that distinct, independent binding sites for Ca^{2+} may explain the range of intracellular Ca^{2+} concentration ($[Ca^{2+}]_i$) that regulates channel opening[5,13]. Over the physiological range of $[Ca^{2+}]_i$, relatively Ca^{2+}-selective site(s) mediate channel regulation. In contrast, the effects of $[Ca^{2+}]_i$ in the millimolar range reflect a lower sensitivity site showing selectivity for Ca^{2+} and Mg^{2+}. Here we define principal structural elements required for each Ca^{2+}-dependent regulatory effect. BK channel α-subunits are encoded by a single *Slo1* gene[16,17], with a functional channel arising from the tetrameric assembly of four α-subunits[18]. Although the transmembrane segments (S1–S6, Fig. 1a) of each α-subunit[17,19] share homology with voltage-gated K^+ channels, each α-subunit uniquely contains an extensive C terminus with four additional hydrophobic segments (S7–S10). The C terminus is probably composed of two modular units, as expression in oocytes of separate messages for S0–S8 and S9–S10 peptides produces channels identical to wild-type BK channels[20]. Whereas the Ca^{2+} bowl is contained within the S9–S10 peptide, the C-terminal structure with the S7–S8 segments contains the RCK domain, a second potential regulatory element (Fig. 1a, b) that exhibits extensive homology with a number of bacterial K^+ channels. The structures of two prokaryotic RCK domains have been determined[12,21] and RCK domains may contain binding sites for a variety of regulatory ligands, including nucleotides[22] and cations[21].

To address the role of the RCK domain in BK channel regulation, we took advantage of the fact that a homologue of *Slo1*, the *Slo3* pH-sensitive K^+ channel, lacks Ca^{2+}-dependent regulation[13,23,24]. We focused on residues near folds in the RCK domain that contribute to nucleotide binding in prokaryotic homologues (Fig. 1c). We were

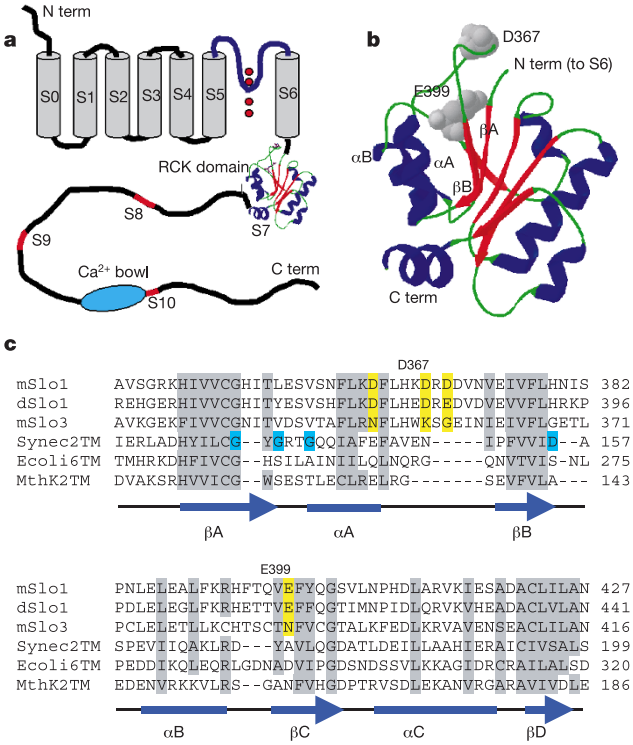

Figure 1 Schematic representation of the Slo1 α-subunit. **a**, The Slo1 α-subunit shares a common transmembrane topology (S1–S6) with voltage-dependent K^+ channels, and contains a unique amino-terminal S0 segment and an extensive cytosolic C-terminal elaboration with hydrophobic segments S8–S10 (red), the Ca^{2+} bowl, and the RCK domain. Segment S7 is contained in the RCK structure[12]. **b**, Structural approximation of the BK channel RCK domain based on the RCK domain of the *E. coli* K^+ channel[12]. The position of the linker between helix αA and βB is uncertain. **c**, Sequence alignment within the RCK domain of Slo1 and Slo3 subunits and three bacterial K^+ channels[12]. Grey indicates semi-conserved residues; blue shows the NAD-binding motif present in some bacterial homologues; and yellow indicates negative residues in *Slo1* that are non-conserved in *Slo3*. mSlo1, mouse BK channel, *Mus musculus* (GenBank accession number: 6754435); dSlo1; *Drosophila* BK channel, *D. melanogaster* (GenBank accession number: 7301192); mSlo3, mouse Slo3 channel, *M. musculus* (GenBank accession number: 6680542); Synec2TM, *Synetchocystis* sp. (GenBank accession number: 7447543); Ecoli6TM, *E. coli* (GenBank accession number: 400124); MthK2TM, *M. thermautotrophicum* (GenBank accession number: 2622639).